Use and misuse of FTIR spectroscopy for studying the bio-oxidation of plastics

Christophe Sandt, Jehan Waeytens, Ariane Deniset-Besseau, Christina Nielsen-Leroux, Agnès Réjasse

Spectrochimica Acta Part A: Molecular and Biomolecular Spectroscopy 258 (2021) 119841

Contents lists available at ScienceDirect

Spectrochimica Acta Part A: Molecular and Biomolecular Spectroscopy

journal homepage: www.elsevier.com/locate/saa

Short Communication

Use and misuse of FTIR spectroscopy for studying the bio-oxidation of plastics

Christophe Sandt [a,*], Jehan Waeytens [b,c], Ariane Deniset-Besseau [b], Christina Nielsen-Leroux [d], Agnès Réjasse [d]

[a] SMIS beamline, Synchrotron Soleil, Orme des Merisiers, BP 48 Saint Aubin, 91192 Gif-sur-Yvette Cedex, France
[b] Université Paris-Saclay, CNRS, Institut de Chimie Physique, UMR 8000, 91405 Orsay, France
[c] Structure et Fonction des Membranes Biologiques, Université libre de Bruxelles, B-1050 Bruxelles, Belgium
[d] Micalis Institute, INRAE (National Research Institute for Agriculture, Food and Environment), AgroParisTech, Université Paris-Saclay, 78350, Jouy-en-Josas, France

HIGHLIGHTS

- Molecular bases for the detection of plastic oxidation by FTIR spectroscopy are reviewed.
- A list of IR absorption peaks for oxidized polyethylene (PE) and polystyrene (PS) and their interpretation is given.
- Spectra of biological contaminants are presented.
- A protocol for cleaning plastics from bio-contaminants while preserving their oxidation state is given.
- Simple methods for analyzing the infrared spectra are suggested.

GRAPHICAL ABSTRACT

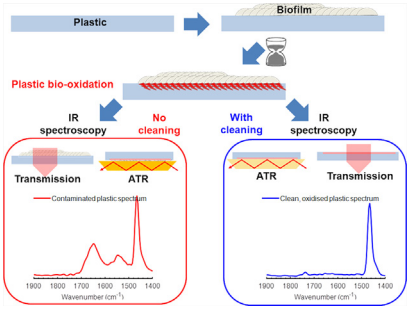

ARTICLE INFO

Article history:
Received 21 January 2021
Received in revised form 15 March 2021
Accepted 12 April 2021
Available online 15 April 2021

Keywords:
FTIR spectroscopy
Plastic biodegradation
Oxidation
Polyethylene
Polystyrene
Insect larvae
Microbial community

ABSTRACT

Due to massive production, inefficient waste collection, and long lives, plastics have become a source of persistent pollution. Biodegradation is explored as an environmentally friendly remediation method for removing plastics from the environment. Microbial and animal biodegradation methods have been reported in the literature for various plastics. Levels of plastic oxidation are often used as an evidence of degradation and can be measured with great sensitivity by Fourier Transform Infrared (FTIR) spectroscopy. FTIR is highly sensitive to the creation of new C—O, C=O and O—H bonds during oxidation. However, many studies reporting the use of FTIR spectroscopy to evidence plastic oxidation confused the spectral signatures of biomass contamination (C—O and C=O from lipids, CONH from proteins, O–H from polysaccharides) with plastic oxidation. Here, based on spectra of oxidized plastic and of probable contaminants, we make recommendations for performing and analyzing FTIR measurements properly.

1. Introduction

Plastics such as polyethylene (PE) and polystyrene (PS) have become a major source of environmental hazard hence a concern for ecosystems, animal and human health. Millions tons of plastics

Abbreviations: ATR, Attenuated Total Reflection; FTIR, Fourier Transform Infrared spectroscopy; IR, infrared; μFTIR, Fourier Transform Infrared microspectroscopy; IRE, Internal Reflection Element; PE, polyethylene; PS, polystyrene; HDPE, High Density Polyethylene; Gm, *Galleria mellonella*.

* Corresponding author.
E-mail address: sandt@synchrotron-soleil.fr (C. Sandt).

https://doi.org/10.1016/j.saa.2021.119841
1386-1425/

are produced every year [1] but only a fraction is collected to be recycled (Plastic Europe Facts 2019). The rest may be collected in landfills or incinerated, but a significant fractions, over 12 million tons per year [2] ends up dispersed in the environment where it can remain for extremely long durations. Plastic wastes often become fragmented under environmental conditions in micro-plastics, defined as particles <5 mm [3]. The plastics and their additives can be toxic, contaminate the food chain and are suspected to cause massive damages to the marine environment. Bioremediation is one solution envisioned to clean the ecosystems, especially those contaminated by micro-plastics that could be near impossible to collect and eliminate. Microbiological biodegradation is the most promising bioremediation method [4–6] but recently biodegradation by the larvae of several insects (*Tenebrio molitor, Galleria mellonella, Plodia interpunctella, Achroia grisella*) have been reported and is explored as an alternative sources of plastic degrading enzymes [7–13]. Characterization of the weak plastic biodegradation can be technically challenging, hindered by the extreme slowness of the process, and often requires the use of multiple methods [4,14]. Fourier Transform Infrared (FTIR) spectroscopy has long been used [15] as an easy and convenient tool to monitor plastic biodegradation since it is exquisitely sensitive to the apparition of C═O, C—O and O—H bonds created during this degradation. However, as noted by Jackson and Mantsch [16], when a technique becomes so widespread, there are pitfalls that become frequently manifested in the literature. FTIR spectroscopy measurements can be performed in many measurement modes that may be suited to different types of plastic and sample environments: in transmission mode for fine powders, thin polymer films or plastic thin sections; in reflection mode for polished bulk samples; in Attenuated Total Reflection (ATR) mode to probe only the surface of bulk samples, powders or films. Spatially resolved information at the micron scale can be obtained in transmission, reflection or ATR modes by IR microspectroscopy either in confocal (μFTIR) or wide-field mode (imaging with detector array) modes. FTIR spectra not only allow detecting the onset and quantitatively evaluate the extent of polymer oxidation but may also be used to understand the degradation mechanism by identifying specific chemical functions formed during oxidation. A diversity of newly formed peaks representing the spectral signature of chemical processes can be identified when following the oxidation of plastics. For polyethylene, $(—CH_2—)_n$, beside the main carbonyl band from ketones (1715–1720 cm^{-1}), FTIR can detect carbonyl bands from aldehydes (1730 cm^{-1}, esters (1740 cm^{-1}), carboxylic acids (1705–1710 cm^{-1}), peroxides (1775 cm^{-1}), peracids R(C═O)OOH (1785 cm^{-1}), peresters R(C═O)OOR (1763 cm^{-1}), and carboxylates (1555 cm^{-1}) [15,17–19]. FTIR can also detect changes in the alkene C═C peak circa 1640 cm^{-1}, and αCH_2 peaks at 1410 and 1415 cm^{-1} (methylene in alpha position of a carbonyl). For polystyrene, $(—CH_2—CHPh—)_n$, that is oxidized by a different mechanism, other peaks are detected, considerably shifted compared to those in oxidized PE, probably due to the conjugation with the benzene ring. Mailhot and Gardette conducted an extensive analysis of photo- and thermally oxidized PS and found the main peaks to be those of ketones (1725 cm^{-1}) and benzoic anhydride (1725 cm^{-1} and 1785 cm^{-1}), benzaldehyde (1704 cm^{-1}), benzophenone (1690 cm^{-1}); they assigned secondary peaks to carboxylates (1553 cm^{-1}), benzoic acid dimers (1698 cm^{-1}) and monomers (1732 cm^{-1}), dibenzoylmethane (1515 and 1605 cm^{-1}), dimeric (1710 cm^{-1}) and monomeric (1753 cm^{-1}) acetic and formic acids [20,21]. Additional bands in the hydroxyl region (3000–3600 cm^{-1}) and in other spectral regions (C—O around 1100–1200 cm^{-1}) can help decipher the oxidation mechanism. The use of FTIR to study biodegradations of various polymers by microbes [7,22–25] or insect larvae [8–12,26] was reviewed by Krueger 2015 [4] and Restrepo Florez 2017 [5]. Even if FTIR appears very attractive, Restrepo Florez [5] noticed that there were some discrepancies in the reported evolutions of the carbonyl bands and that this could arise from different degradation mechanisms. In some cases we suggest it could also result from improper measurements or analysis of FTIR data. We critically reviewed several articles reporting the use of FTIR spectroscopy to study the biodegradation of plastics, mainly the biodegradation of PE and PS. We noticed shortcomings in some of the publications examined that could potentially lead to false conclusions. We identify two types of protocols used for evaluating microbial or larval PE oxidation: measurement of plastic films in direct contact with environmental microbes and biofilms, larval microbiota or larval gut as reported in [7,12,24,27–29]; measurement of plastic in larval frass with or without extraction as reported in [9–11,30,31]. We replicated both protocols and analyzed the resulting PE by ATR-FTIR spectroscopy and hyperspectral FTIR imaging, and report our observations thereafter. We make recommendations for the proper use of FTIR for assessing plastic biodegradation.

2. Materials and methods

2.1. FTIR spectroscopy analysis of standards

Galleria mellonella (Gm) larvae were produced on site in the insectarium at INRAE Micalis Institute in Jouy-en-Josas, France. Gm eggs were hatched at 27 °C. The larvae were reared on commercially purchased beeswax and pollen (La Ruche Roannaise, Roanne, France) which were also used in the feeding experiments and as standards for the spectral analyses.

Last stage L6 larvae were starved for 24 h at 27 °C in individual boxes then fed for 4 to 10 days either with PE (pieces cut from commercial plastic bags), or with beeswax. Larvae ate 0.55 mg of PE or 13 mg of beeswax per day in average. Larval frass and silk were collected directly from the Gm boxes after 4 days for frass and 10 days for silk, stored at −80 °C, lyophilized for 24 h, and used for the spectral analyses.

PE films were pressed from PE powder (purchased from Merck) and thermally oxidized in an oven at 140 °C for 22 h. Photo-oxidized PE was collected from a piece of hazard-warning tape that had been exposed to sun and outside conditions for several years.

The infrared spectra were collected in ATR mode either at Paris-Saclay University with a Vertex 70 FTIR spectrometer (Bruker, Marne-la-Vallée, France) equipped with a MCT detector, or at SOLEIL synchrotron with a Nicolet 5700 FTIR spectrometer (ThermoFisher Scientific, Courtaboeuf, France) equipped with a DTGS detector. Spectra were collected between 400 and 4000 cm^{-1} at 4 cm^{-1} resolution with 100 to 256 co-added scans. Both instruments were equipped with single-bounce diamond Internal Reflection Element (IRE).

2.2. Incubation of PE films with Gm digestive tube

PE plastic bags were cut in 3 cm × 6 cm triangular pieces and sterilized on each side by UV light at 254 nm during 10 min. L6 larvae were starved for 24 h and dissected to extract their digestive tube. The larvae were cut longitudinally from the ventral side, and the skin spread with pins, the fat body tissues were removed, and the digestive tube was removed from the head to the anus. The digestive tubes were opened longitudinally so that the inner part of the gut could be placed in direct contact with the PE films. Two complete digestive tubes were placed on each of the PE pieces, then deposited in Petri dishes and incubated at 27 °C in humid atmosphere for 24 h. The PE pieces were then cleaned by a specifically developed protocol.

2.3. Plastic cleaning protocol

Pieces of PE films were rinsed and shaken in deionised water, followed by another bath in hot water at 60 °C, then rinsed in 50% ethanol at 60 °C, then washed 5 times for 5 min in NaOH 1 M at room temperature in an ultrasonic bath, and finally rinsed in distilled water and dried at room temperature. Clean PE films without contact with Gm gut were used as control.

2.4. Analysis of PE films by hyperspectral FTIR imaging

The PE films were measured by hyperspectral FTIR imaging on a Cary 620 infrared microscope (Agilent, Courtaboeuf, France) equipped with a 128 × 128 pixels "Lancer" Focal Plane Array (FPA) detector, and coupled to a Cary 670 FTIR spectrometer. Hyperspectral images were measured in transmission in the standard magnification mode with a 15 × magnification, 0.65 numerical aperture (NA) Schwarzschild objective and matching condenser giving a field of view of 704 × 704 μm^2, and a projected pixel size of 5.5 × 5.5 μm^2. Mosaic images were measured by assembling multiple FPA tiles (98,304 to 196,608 spectra). The hyperspectral images were recorded between 900 and 3900 cm^{-1} at 8 cm^{-1} resolution, with 256 co-added scans for background and 128 co-added scans for sample.

The hyperspectral images were used for evaluating the extent of PE film oxidation and contamination by computing specific peak areas and peak area ratios in the Quasar software [32,33]. PE oxidation was evaluated by the carbonyl index: the area of the carbonyl ν C=O band (1650–1780 cm^{-1}) divided by the area of the methylene δ C-H band (1440–1485 cm^{-1}). Protein contamination was evaluated by the area of the amide I band (1595–1705 cm^{-1}) after subtraction of a linear baseline between the peak edges. For the control samples, the integrated area of the amide I band was 0.2 ± 0.6 (min: −1.4, max 4.0) Arbitray Unit (AU). Baseline deviation, interference fringes, measurement noise and water vapor signal may explain the variations and the occurrence of negative values. For PE samples cleaned after contact with Gm gut, the integrated amide I band area varied between −0.7 and 27 AU. The typical amide I shape became recognizable at values of around 0.6 AU. We thus selected the value of 0.6 AU as a threshold to separate clean and contaminated PE. The clean surface fraction was measured as the ratio of the number of pixels with protein band area below and above the 0.6 AU threshold.

3. Results and discussion

We first attempted to measure the oxidation of PE particles directly in the larval frass. Fig. 1A shows the spectra of Gm frass from PE-fed larvae and from beeswax-fed larvae, and the spectrum of strongly, thermally-oxidized PE. All spectra present C=O peaks at around 1740 cm^{-1}, C—O peaks between 1100 and 1200 cm^{-1}. O—H peaks (3400–3600 cm^{-1}) can be seen in the frass spectra from both PE-fed and beeswax-fed larvae. The O—H peak must not be confused with the N–H peak located at 3300 cm^{-1} (recognizable by its position and pointed shape) as in reference [27] where the N—H peak was taken as evidence for polyethylene glycol formation. CH_2 peaks are found even in the spectra of beeswax-fed larval frass and cannot be used to detect the PE. Both beeswax-fed and PE-fed larval-frass spectra show strong peaks of proteins (1480–1700 cm^{-1}) and polysaccharides (900–1180 cm^{-1}), probably from pollen (Fig. 1B) even if the larvae had been starved for 24 h before switching to the beeswax or PE diets. The fact that pollen and beeswax can be detected in feces after 120 h without eating pollen and beeswax shows that a 24 h starvation period is not sufficient to eliminate the earlier content of the larval gut. A 24 h starvation period is sometime reported in the literature but most groups report no prior starvation period. Importantly, both beeswax-fed and PE-fed larval frass spectra present strong methyl, methylene, carbonyl and carbon–oxygen peaks from the different contaminants overlapping the position of C—H, C=O and C—O bands in oxidized PE.

Fig. 1B shows typical spectra from possible contaminants: pollen, beeswax, Gm silk, Gm gut extract. Beeswax, Gm gut, pollen and Gm frass all contain strong carbonyl peaks circa 1740 cm^{-1} (C=O from esters) which intensity could totally obscure that of oxidized PE. Beeswax presents two C=O peaks at 1720 and at 1736 cm^{-1} that could interfere with the interpretation of the complex C=O peak from oxidized PE. It is thus impossible to evaluate plastic oxidation in the presence of fats in frass using the carbonyl peak. Silk is produced by the larvae for cocoon construction and is frequently found as a contaminant on the PE films having been in contact with the larvae. Silk can also be used for demonstrating how protein contamination (from other types of proteins) would influence the PE spectrum. Protein contamination could happen from larval silk, from the gut peritrophic matrix, from gut cells or other proteins from food or metabolism, or from microbial biofilm attached to the plastic. Protein spectra are dominated by the amide I and amide II bands centered at 1650 and 1545 cm^{-1}. Due to their intensity and recognizable shapes, protein amide bands are good indicators of biological contamination. Unfortunately such peaks are frequently observed in biodegraded plastic spectra reported in the literature [11,12,27,28,30,31,34], and clearly evidence the contamination of the plastic by protein residues. Beside C=O peaks, contaminants present other absorption bands that can prevent the evaluation of oxidation: O—H, C—H and C—O peaks. Pollen, beeswax and gut tissue spectra also have other strong C—H peaks between 1400 and 1450 cm^{-1} and C—O peaks between 900 and 1200 cm^{-1} that would totally hide the weaker C—H scissoring peaks from αCH_2 and C—O peaks from PE oxidation. Microbial biofilms produce exopolysaccharides in their extracellular matrix that have strong C—O and C—C absorption peaks between 900 and 1180 cm^{-1} potentially hiding weaker C—O peaks from PE oxidation. It is therefore impossible to properly assess plastic oxidation when PE is contaminated by larva tissues, microbial biofilm or directly in frass. In theory subtracting the contaminant spectrum could eliminate the confounding signals but this is nearly impossible in practice.

Another technique frequently reported in the literature is to incubate plastic films with microbial biofilms or gut extracts, and to evaluate the oxidation of the film after a period of hours to months. We replicated this by measuring the spectral signature of PE films in contact with dissected Gm larva gut for 24 h. The findings may also apply to PE in contact with microbial biofilms. The PE films were cleaned by the specifically developed protocol reported in the Materials & Methods section. In Fig. 1C we report the IR spectra of the surface of the initial pristine PE, of PE film bio-oxidized after 24 h in contact with the Gm larva gut, and of strongly thermally-oxidized PE (140 °C, 22 h). Thermally-oxidized PE exhibits a clear, complex carbonyl band centered at 1710 cm^{-1} with shoulders at 1735 and 1772 cm^{-1} and several other peaks related to PE oxidation at 1415 and 1420 (δ C—H of αCH_2) and 1172 cm^{-1} (C—O). Biodegradation will generally cause much slower oxidation than thermal oxidation, and may affect mostly the surface of the film in contact with enzymes, thus carbonyl band intensity will be much weaker. In the IR spectrum of bio-oxidized PE after 24 h in contact with Gm gut, the carbonyl band is nearly 150 times weaker than in the 22 h thermally-oxidized sample (Fig. 1C). The weak oxidation signal can be easily eclipsed by the bio-contaminant signal reported in Fig. 1B. Furthermore, it should be noted that 'natural' oxidation may already be present at discrete, micron-sized, locations in control plastic

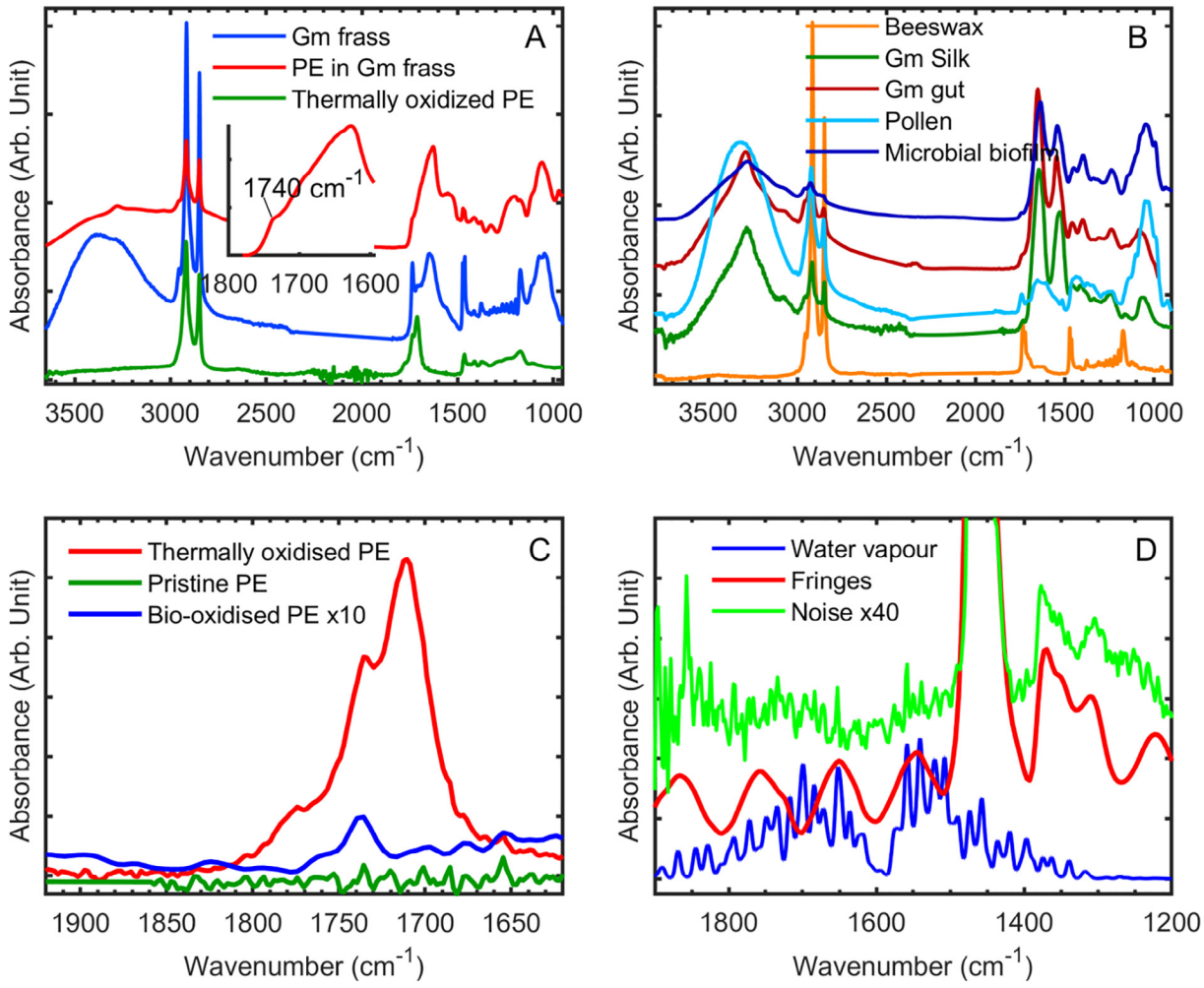

Fig. 1. FTIR spectra of PE and various confounding signals. A) ATR-FTIR spectra of Gm frass (from larvae fed a beeswax and pollen diet), of PE fragments measured directly in Gm frass, and of strongly oxidized PE. All PE peaks are overlapped by stronger peaks from biological molecules in the frass. Insert: zoom on the amide I region of the PE in frass spectrum to point out the shoulder of the C=O peak at 1740 cm^{-1}. B) ATR-FTIR spectra from possible bio-contaminants: Gm gut tissue, pollen, beeswax, Streptomyces microbial biofilm and silk. The C—O (1170 cm^{-1}) and C=O peaks (1700–1760 cm^{-1}) in oxidized PE can be totally obscured by stronger peaks from Gm gut tissue, pollen or beeswax. C) ATR-FTIR spectra of pristine PE, bio-oxidized PE (24 h in contact with Gm gut) and thermally oxidized PE (140 °C, 22 h) in the C=O region evidencing the 150 times weaker C=O from bio-oxidation (the bio-oxidized PE spectrum was multiplied by 10). D) Other confounding factors: spectrum of a PE film with interference fringes, water vapor spetrum and noisy ATR spectrum; interference fringes and O-H peaks are found at the C=O peak position. All spectra were normalized and offset for clarity.

samples, thus each sample should be evaluated before and after bio-oxidation.

In addition to bio-contaminants, other confounding factors may hide or alter the carbonyl band, or appear as a spurious carbonyl band. Fig. 1D presents a series of PE film spectra with interference fringes, noise, and a spectrum of water vapor. Interference fringes occur in films because internal reflections of IR beam. This creates constructive and destructive interferences that translate in a sinusoid baseline which may alter C=O peak shape, position, intensity, and area. Water vapor presents over 40 sharp IR absorption peaks in the 1300–2000 cm^{-1} range, one at 1735 cm^{-1} and one at 1635 cm^{-1} that may respectively affect or appear as the carbonyl C=O band and the alkene C=C band. Water vapor signal may appear when the infrared spectrometer dry-air or nitrogen purge is not stable over time. Although it is less of a problem with modern instruments that provide very good signal to noise ratios, measurement noise can still be problematic in the ATR mode due to the small sample volume probed and to IR radiation losses due to the ATR IRE. Noise can hinder the detection of C=O peaks, create spurious peaks, alter peak shape and position and lower the accuracy of peak intensity evaluation.

Thus, in order to properly use FTIR spectroscopy or μFTIR to evidence PE film oxidation, it is necessary to verify the absence of oxidation before the experiment, to perform a thorough cleaning of the PE films, and, after, to verify the absence of bio-contamination by looking at the presence of protein and lipid peaks. We recommend using the cleaning protocol described in the Experimental section: multiple serial rinsing of PE in deionised water and in hot water (60 °C) to remove proteins, in hot ethanol (60 °C) to remove lipids, in NaOH with ultrasonication to solubilize carboxylic acids, and in deionised water to eliminate NaOH, and finally drying at room temperature. The cleaning protocol had only minute impact on the oxidation level of the PE films: the carbonyl index of the PE films was −0.0009 ± 0.1050 (n = 65536) before cleaning and −0.0030 ± 0.0069 (n = 94699) after cleaning, showing that oxidation was undetected in both cleaned and non-cleaned PE films. The cleaning protocol was then used to clean the PE films after 24 h in contact with dissected Gm guts. Hyperspectral FTIR imaging of the cleaned films showed that 99.5 to 99.9% of the film surface were free from protein contaminants. Protein contamination was only detected at few, micron-sized, discrete locations. Films in contact for longer periods were more contaminated.

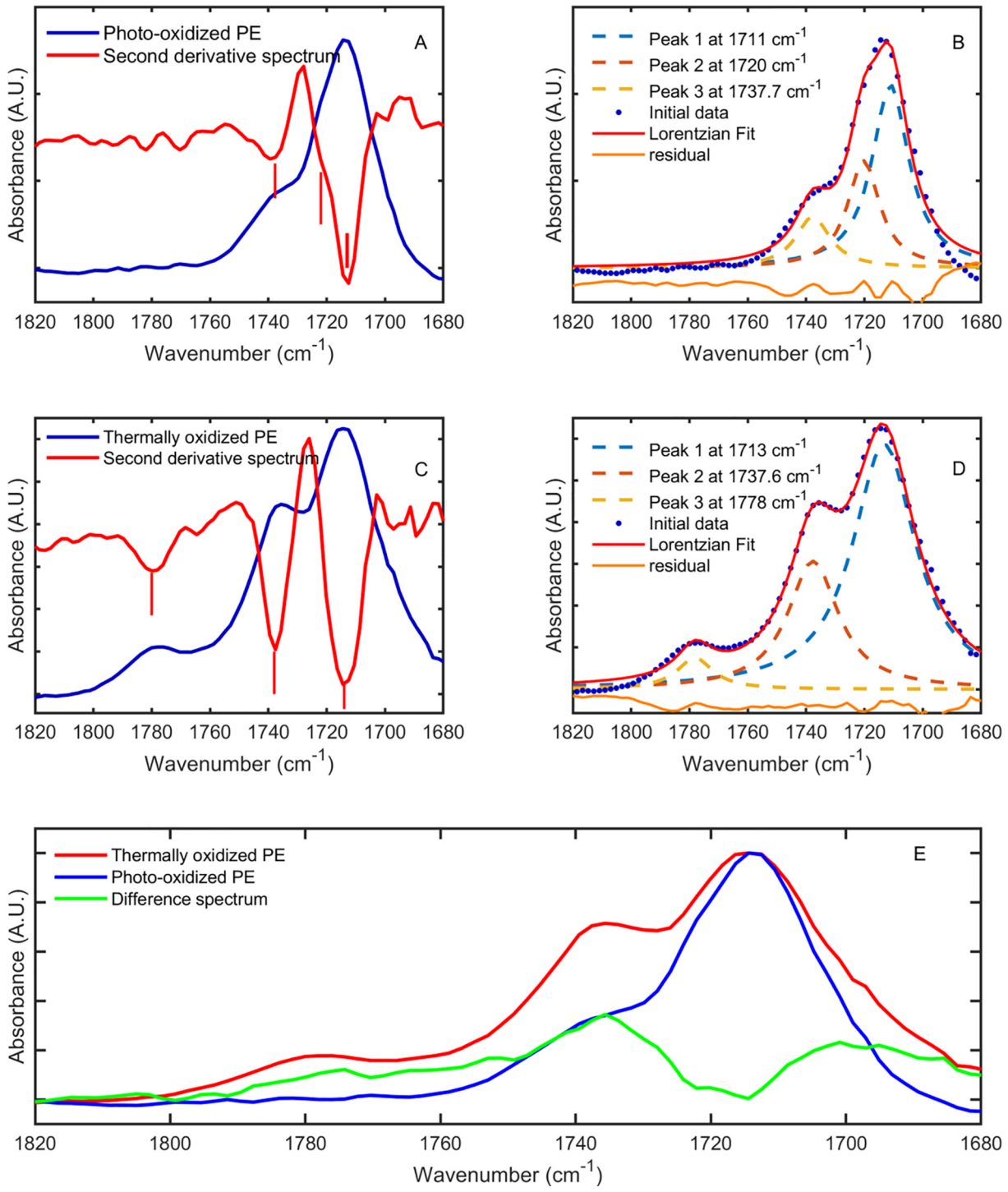

Fig. 2. Example of use of second derivative, curve-fitting, and difference spectroscopy for analyzing PE oxidation. Thermally oxidized and photo-oxidized PE samples were used. The complex carbonyl band of oxidized PE was analyzed by second derivative (A and C) and computed with a Savitzky-Golay filter (9 points window, 2nd order polynomial). The curve-fitting analysis (B and D) performed by least-square minimization with an in-house script based on the Python lmfit package [37] in the Quasar software. The second derivative spectrum was used to find the peaks (appearing as narrower negative peaks), marked by thin lines, inside the larger carbonyl band. The curve-fitting analysis was used for decomposing the carbonyl band in its main components and find their relative contributions. For both samples, we decomposed the carbonyl band in 3 peaks. A) and B) the photo-oxidized PE was fitted with 3 Lorentzian peaks at 1711 cm^{-1} (ketones), 1720 cm^{-1} (aldehydes) and 1737.7 cm^{-1} (esters) – (tentative assignments). C) and D) thermally oxidized PE: the carbonyl band was fitted with 3 Lorentzian peaks at 1713 cm^{-1} (ketones), 1737.6 cm^{-1} (esters), and 1778 cm^{-1} (peroxides) –tentative assignments. E) Difference spectroscopy for comparing the oxidation mechanisms. The spectra of thermally oxidized (TOx) PE and photo-oxidized (POx) PE were normalized on the ketone peak at 1712 cm^{-1} and subtracted. The resulting TOx – POx difference spectrum shows peaks at about 1780 cm^{-1} (peroxides), 1737 cm^{-1} (esters), revealing that the thermally oxidized PE contains more esters and peroxides than the photo-oxidized PE. The round peak near 1700 cm^{-1} may come the difference in width between the ketone peaks, the TOx-PE peak being wider suggests more conformational freedom or more diverse oxidation sites; or from the optical dispersion effect in strong peak feet.

It could also be more appropriate to measure the IR spectra in the surface sensitive Attenuated Total Reflection (ATR) mode rather than the transmission mode since it can be expected that PE oxidation by gut extracts or by microbial biofilms will happen mostly at the surface of the PE film or particles.

The spectra should preferably be displayed in absorbance mode (making peak height linearly proportional to concentration) and normalized on a relevant band (such as the —CH_2— bending at 1465 cm^{-1}) to facilitate interpretation and comparisons. The oxidation should be assessed by using an objective marker such as the carbonyl index (area ratio of the carbonyl band and that of the methylene group at 1465 cm^{-1}) or more sensitive indices [35]. For example, the carbonyl indices of the thermally oxidized PE, photo-oxidized PE and pristine PE were respectively 4.07, 0.37 and −0.63.

The computation of second derivative spectra should be used to deconvolute the complex carbonyl C═O peak to identify its multiple components and elucidate the oxidation mechanism as shown in Fig. 2A and C. The information gathered from the second derivative was used to perform curve-fitting analyses of the carbonyl band and to find the relative contributions of the peaks (Fig. 2B and D).

Since FTIR is a non-destructive technique it could theoretically be used to follow plastic degradation by measuring the same sample at different times during the oxidation process to monitor its kinetic. However, this would require cleaning before and sterilizing after each measurement.

The technique of "difference spectroscopy" could be useful for studying spectral changes by systematically subtracting the spectrum from unaltered sample from that of the oxidized sample to reveal the spectral differences and eliminate unchanging peaks. It can be performed systematically to follow changes at every step of an oxidation kinetic [36]. Here, we used spectra from photo-oxidized PE and thermally-oxidized PE to demonstrate difference spectroscopy (Fig. 2E). The thermally oxidized PE exhibit stronger carbonyl peaks at 1780 cm^{-1} (peroxides, absent in photo-oxidized PE) and 1737 cm^{-1} (esters, weaker in photo-oxidized PE). The spectra were normalized on the ketone peak, assuming the ketone intensity was the same in both spectra.

4. Conclusion

FTIR spectroscopy in its various modes can be a useful tool to detect, follow, quantify and understand plastic bio-oxidation but it requires a good understanding of the technique, adequate sampling method (ATR must be preferred for evaluating the oxidation at the surface of plastic films), suitable sample preparation (cleaning to remove biocontaminants without altering the plastic oxidation state), and a correct analysis for interpreting the mechanism of oxidation. IR spectra from protein and fat contaminants may be confounded for oxidation signs and must thus be eliminated before qualitatively or quantitatively assessing the plastic oxidation.

Funding Sources

The authors acknowledge the Synchrotron SOLEIL for provision of FTIR microspectroscopy equipment. The authors also acknowledge the INRAE-MICA department for the general support to CNLR and AR. Funding for instrumentation was provided by synchrotron SOLEIL and the DIM-ACAV grant of the Ile-de-France region.

CRediT authorship contribution statement

Christophe Sandt: Conceptualization, Formal analysis, Investigation, Validation, Visualization, Supervision, Writing - original draft. **Jehan Waeytens:** Methodology, Formal analysis, Writing - review & editing. **Ariane Deniset-Besseau:** Investigation, Writing - review & editing. **Christina Nielsen-Leroux:** Writing - review & editing. **Agnès Réjasse:** Conceptualization, Investigation, Writing - review & editing.

Declaration of Competing Interest

The authors declare that they have no known competing financial interests or personal relationships that could have appeared to influence the work reported in this paper.

References

[1] R. Geyer, J.R. Jambeck, K.L. Law, Production, use, and fate of all plastics ever made, Sci. Adv. 3 (7) (2017) e1700782, https://doi.org/10.1126/sciadv.1700782.
[2] J.C. Prata, A.L.P. Silva, J.P. da Costa, C. Mouneyrac, T.R. Walker, A.C. Duarte, T. Rocha-Santos, Solutions and integrated strategies for the control and mitigation of plastic and microplastic pollution, Int. J. Environ. Res. Public Health. 16 (2019) 2411, https://doi.org/10.3390/ijerph16132411.
[3] H.S. Auta, C.U. Emenike, S.H. Fauziah, Distribution and importance of microplastics in the marine environmentA review of the sources, fate, effects, and potential solutions, Environ. Int. 102 (2017) 165–176, https://doi.org/10.1016/j.envint.2017.02.013.
[4] M.C. Krueger, H. Harms, D. Schlosser, Prospects for microbiological solutions to environmental pollution with plastics, Appl. Microbiol. Biotechnol. 99 (21) (2015) 8857–8874, https://doi.org/10.1007/s00253-015-6879-4.
[5] J.M. Restrepo-Flórez, A. Bassi, M.R. Thompson, Microbial degradation and deterioration of polyethylene - A review, Int. Biodeterior. Biodegrad. 88 (2014) 83–90, https://doi.org/10.1016/j.ibiod.2013.12.014.
[6] B.T. Ho, T.K. Roberts, S. Lucas, An overview on biodegradation of polystyrene and modified polystyrene: the microbial approach, Crit. Rev. Biotechnol. 38 (2) (2018) 308–320, https://doi.org/10.1080/07388551.2017.1355293.
[7] J. Yang, Y.u. Yang, W.-M. Wu, J. Zhao, L. Jiang, Evidence of polyethylene biodegradation by bacterial strains from the guts of plastic-eating waxworms, Environ. Sci. Technol. 48 (23) (2014) 13776–13784, https://doi.org/10.1021/es504038a.
[8] S.S. Yang, W.M. Wu, A.M. Brandon, H.Q. Fan, J.P. Receveur, Y. Li, Z.Y. Wang, R. Fan, R.L. McClellan, S.H. Gao, D. Ning, D.H. Phillips, B.Y. Peng, H. Wang, S.Y. Cai, P. Li, W.W. Cai, L.Y. Ding, J. Yang, M. Zheng, J. Ren, Y.L. Zhang, J. Gao, D. Xing, N. Q. Ren, R.M. Waymouth, J. Zhou, H.C. Tao, C.J. Picard, M.E. Benbow, C.S. Criddle, Ubiquity of polystyrene digestion and biodegradation within yellow mealworms, larvae of Tenebrio molitor Linnaeus (Coleoptera: Tenebrionidae), Chemosphere. 212 (2018) 262–271, https://doi.org/10.1016/j.chemosphere.2018.08.078.
[9] S.-S. Yang, A.M. Brandon, J.C. Andrew Flanagan, J. Yang, D. Ning, S.-Y. Cai, H.-Q. Fan, Z.-Y. Wang, J. Ren, E. Benbow, N.-Q. Ren, R.M. Waymouth, J. Zhou, C.S. Criddle, W.-M. Wu, Biodegradation of polystyrene wastes in yellow mealworms (larvae of Tenebrio molitor Linnaeus): Factors affecting biodegradation rates and the ability of polystyrene-fed larvae to complete their life cycle, Chemosphere 191 (2018) 979–989, https://doi.org/10.1016/j.chemosphere.2017.10.117.
[10] A.M. Brandon, S.-H. Gao, R. Tian, D. Ning, S.-S. Yang, J. Zhou, W.-M. Wu, C.S. Criddle, Biodegradation of Polyethylene and Plastic Mixtures in Mealworms (Larvae of *Tenebrio molitor*) and Effects on the Gut Microbiome, Environ. Sci. Technol. 52 (11) (2018) 6526–6533, https://doi.org/10.1021/acs.est.8b02301.
[11] H. Kundungal, M. Gangarapu, S. Sarangapani, A. Patchaiyappan, S.P. Devipriya, Efficient biodegradation of polyethylene (HDPE) waste by the plastic-eating lesser waxworm (Achroia grisella), Environ. Sci. Pollut. Res. Int. 26 (18) (2019) 18509–18519, https://doi.org/10.1007/s11356-019-05038-9.
[12] L. Ren, L. Men, Z. Zhang, F. Guan, J. Tian, B. Wang, J. Wang, Y. Zhang, W. Zhang, Biodegradation of polyethylene by Enterobacter sp. D1 from the Guts of Wax Moth Galleria mellonella, Int. J. Environ. Res. Public Health. 16 (11) (2019) 1941, https://doi.org/10.3390/ijerph16111941.
[13] H.G. Kong, H.H. Kim, J.-H. Chung, JeHoon Jun, S. Lee, H.-M. Kim, S. Jeon, S.G. Park, J. Bhak, C.-M. Ryu, The Galleria mellonella Hologenome supports microbiota-independent metabolism of long-chain hydrocarbon beeswax, Cell Rep. 26 (9) (2019) 2451–2464.e5, https://doi.org/10.1016/j.celrep.2019.02.018.
[14] N. Lucas, C. Bienaime, C. Belloy, M. Queneudec, F. Silvestre, J.-E. Nava-Saucedo, Polymer biodegradation: mechanisms and estimation techniques - A review, Chemosphere 73 (4) (2008) 429–442, https://doi.org/10.1016/j.chemosphere.2008.06.064.
[15] A.-C. Albertsson, S.O. Andersson, S. Karlsson, The mechanism of biodegradation of polyethylene, Polym. Degrad. Stab. 18 (1) (1987) 73–87, https://doi.org/10.1016/0141-3910(87)90084-X.
[16] M. Jackson, H.H. Mantsch, The use and misuse of ftir spectroscopy in the determination of protein structure, 30 (1995) 95–120.
[17] J.P. Luongo, Infrared study of oxygenated groups formed in polyethylene during oxidation, J. Polym. Sci. 42 (1960) 139–150, https://doi.org/10.1002/pol.1960.1204213916.

[18] F.M. Rugg, J.J. Smith, R.C. Bacon, Infrared spectrophotometric studies on polyethylene. II. Oxidation, J. Polym. Sci. 13 (72) (1954) 535–547, https://doi.org/10.1002/pol.1954.120137202.
[19] M. Da Cruz, L. Van Schoors, K. Benzarti, X. Colin, Thermo-oxidative degradation of additive free polyethylene. Part I. Analysis of chemical modifications at molecular and macromolecular scales, J. Appl. Polym. Sci. 133 (18) (2016) n/a–n/a, https://doi.org/10.1002/app.v133.1810.1002/app.43287.
[20] B. Mailhot, J.L. Gardette, P. Photooxidation, 1. Identification of the IR-absorbing photoproducts formed at short and long wavelengths, Macromolecules 25 (1992) 4119–4126, https://doi.org/10.1021/ma00042a012.
[21] Y. Israeli, J. Lacoste, J. Lemaire, R.P. Singh, S. Sivaram, Photo- and thermoinitiated oxidation of high-impact polystyrene. I. Characterization by FT-IR spectroscopy, J. Polym. Sci. Part APolym. Chem. 32 (1994) 485–493, https://doi.org/10.1002/pola.1994.080320310.
[22] J.C. Biffinger, D.E. Barlow, R.K. Pirlo, D.M. Babson, L.A. Fitzgerald, S. Zingarelli, L. J. Nadeau, W.J. Crookes-Goodson, J.N. Russell, A direct quantitative agar-plate based assay for analysis of Pseudomonas protegens Pf-5 degradation of polyurethane films, Int. Biodeterior. Biodegrad. 95 (2014) 311–319, https://doi.org/10.1016/j.ibiod.2014.09.005.
[23] A. Corti, S. Muniyasamy, M. Vitali, S.H. Imam, E. Chiellini, Oxidation and biodegradation of polyethylene films containing pro-oxidant additives: Synergistic effects of sunlight exposure, thermal aging and fungal biodegradation, Polym. Degrad. Stab. 95 (6) (2010) 1106–1114, https://doi.org/10.1016/j.polymdegradstab.2010.02.018.
[24] D. Hadad, S. Geresh, A. Sivan, Biodegradation of polyethylene by the thermophilic bacterium Brevibacillus borstelensis, J. Appl. Microbiol. 98 (5) (2005) 1093–1100, https://doi.org/10.1111/j.1365-2672.2005.02553.x.
[25] C.N. Muhonja, H. Makonde, G. Magoma, M. Imbuga, Biodegradability of polyethylene by bacteria and fungi from Dandora dumpsite Nairobi-Kenya, PLoS One. 13 (2018), https://doi.org/10.1371/journal.pone.0198446.
[26] Y.u. Yang, J. Yang, W.-M. Wu, J. Zhao, Y. Song, L. Gao, R. Yang, L. Jiang, Biodegradation and Mineralization of Polystyrene by Plastic-Eating Mealworms: Part 1. Chemical and Physical Characterization and Isotopic Tests, Environ. Sci. Technol. 49 (20) (2015) 12080–12086, https://doi.org/10.1021/acs.est.5b02661.
[27] P. Bombelli, C.J. Howe, F. Bertocchini, Polyethylene bio-degradation by caterpillars of the wax moth Galleria mellonella, Curr. Biol. 27 (8) (2017) R292–R293, https://doi.org/10.1016/j.cub.2017.02.060.
[28] S. Bonhomme, A. Cuer, A.-M. Delort, J. Lemaire, M. Sancelme, G. Scott, Environmental biodegradation of polyethylene, Polym. Degrad. Stab. 81 (3) (2003) 441–452, https://doi.org/10.1016/S0141-3910(03)00129-0.
[29] B. Nowak, J. Pająk, M. Drozd-Bratkowicz, G. Rymarz, Microorganisms participating in the biodegradation of modified polyethylene films in different soils under laboratory conditions, Int. Biodeterior. Biodegrad. 65 (6) (2011) 757–767, https://doi.org/10.1016/j.ibiod.2011.04.007.
[30] H. Kundungal, M. Gangarapu, S. Sarangapani, A. Patchaiyappan, S.P. Devipriya, Role of pretreatment and evidence for the enhanced biodegradation and mineralization of low-density polyethylene films by greater waxworm, Environ. Technol. (United Kingdom). 42 (5) (2021) 717–730, https://doi.org/10.1080/09593330.2019.1643925.
[31] Y.u. Lou, P. Ekaterina, S.-S. Yang, B. Lu, B. Liu, N. Ren, P.-X. Corvini, D. Xing, Biodegradation of Polyethylene and Polystyrene by Greater Wax Moth Larvae (Galleria mellonella L.) and the Effect of Co-diet Supplementation on the Core Gut Microbiome, Environ. Sci. Technol. 54 (5) (2020) 2821–2831, https://doi.org/10.1021/acs.est.9b07044.
[32] J. Demšar, T. Curk, A. Erjavec, T. Hočevar, M. Milutinovič, M. Možina, M. Polajnar, M. Toplak, A. Starič, M. Stajdohar, L. Umek, L. Zagar, J. Zbontar, M. Zitnik, B. Zupan, Orange data mining toolbox in python, J. Mach. Learn. Res. 14 (2013) 2349–2353, accessed March 8, 2017.
[33] M. Toplak, G. Birarda, S. Read, C. Sandt, S.M. Rosendahl, L. Vaccari, J. Demšar, F. Borondics, Infrared orange: connecting hyperspectral data with machine learning, Synchrotron Radiat. News. 30 (4) (2017) 40–45, https://doi.org/10.1080/08940886.2017.1338424.
[34] B.-Y. Peng, Y. Su, Z. Chen, J. Chen, X. Zhou, M.E. Benbow, C.S. Criddle, W.-M. Wu, Y. Zhang, Biodegradation of Polystyrene by Dark (Tenebrio obscurus) and Yellow (Tenebrio molitor) Mealworms (Coleoptera: Tenebrionidae), Environ. Sci. Technol. 53 (9) (2019) 5256–5265, https://doi.org/10.1021/acs.est.8b06963.
[35] C. Rouillon, P.O. Bussiere, E. Desnoux, S. Collin, C. Vial, S. Therias, J.L. Gardette, Is carbonyl index a quantitative probe to monitor polypropylene photodegradation?, Polym. Degrad. Stab. 128 (2016) 200–208, https://doi.org/10.1016/j.polymdegradstab.2015.12.011.
[36] M. Gardette, A. Perthue, J.-L. Gardette, T. Janecska, E. Földes, B. Pukánszky, S. Therias, Photo- and thermal-oxidation of polyethylene: Comparison of mechanisms and influence of unsaturation content, Polym. Degrad. Stab. 98 (11) (2013) 2383–2390, https://doi.org/10.1016/j.polymdegradstab.2013.07.017.
[37] M. Newville, T. Stensitzki, D.B. Allen, A. Ingargiola, LMFIT: Non-linear least-square minimization and curve-fitting for python, (2014). https://doi.org/10.5281/ZENODO.11813.